



**Ramakrishna Mission Residential College (Autonomous)**  
Kolkata 700103, WB, India

---

**Collaborative research in coordination chemistry of organic radicals**  
**Number 10**

**Institute 1: Ramakrishna Mission Residential College (Autonomous)**

**Concerned Faculty: Dr. Prasanta Ghosh, Dept of Chemistry**

**&**

**Institute 2: Max-Planck-Institut für Chemische Energiekonversion**

Stiftstrasse 34 - 36 / D - 45470 Mülheim an der Ruhr

**Concerned Scientist: Dr Thomas Weyhermüller**

**Period of Investigation: 02-01-2016 to 10-06-2016**

**Project: Analyses of copper-cuprizone and analogues**

**Output:** The result was published in a journal of international repute

**Publication: Molecular and electronic structures of copper-cuprizone and analogues**

Suman Kundu, Amiya Mondal, Thomas Weyhermüller, Stephen Sproules and Prasanta Ghosh\*

*Inorg. Chim. Acta*, 2016, 451, 23-30.

-----  
Dr. Prasanta Ghosh

-----  
Dr Thomas Weyhermüller





Contents lists available at ScienceDirect

Inorganica Chimica Acta

journal homepage: [www.elsevier.com/locate/ica](http://www.elsevier.com/locate/ica)

Research paper

## Molecular and electronic structures of copper-cuprizone and analogues

Suman Kundu<sup>a</sup>, Amiya Mondal<sup>a</sup>, Thomas Weyhermüller<sup>b</sup>, Stephen Sproules<sup>c</sup>, Prasanta Ghosh<sup>a,\*</sup><sup>a</sup> Department of Chemistry, R. K. Mission Residential College, Narendrapur, Kolkata 700103, India<sup>b</sup> Max-Planck-Institut für Chemische Energiekonversion, Stiftstrasse 34-36, D-45470 Mülheim an der Ruhr, Germany<sup>c</sup> WestCHEM, School of Chemistry, University of Glasgow, Glasgow G12 8QQ, United Kingdom

## ARTICLE INFO

## Article history:

Received 24 February 2016

Received in revised form 24 May 2016

Accepted 28 June 2016

Available online 29 June 2016

## Keywords:

Dinuclear copper(II) complex

Copper cuprizone

Electronic structure

DFT calculations

## ABSTRACT

A paramagnetic dinuclear copper(II) complex,  $[\text{Cu}^{\text{II}}(\text{L}^-)\text{Cl}]_2$  (**1**) while  $\text{LH} = (E)$ -1,2-diphenyl-2-(2-(pyridine-2-yl)hydrozono)ethanone, an analogue of mono-hydrazone cuprizone ( $\text{L}_{\text{mcpz}}\text{H}_2$ ), was isolated and substantiated by spectra, single crystal X-ray structure determination, unrestricted density functional theory (DFT) calculations and inter alia. Magnetic susceptibility measurement and EPR spectra confirmed the triplet state of **1** above 30 K because of two paramagnetic copper(II) centers. Unrestricted DFT calculations on copper cuprizone species with doublet spin state established similar electronic features and disclosed that bis-deprotonated NN-chelation,  $[\text{Cu}(\text{L}_{\text{mcpz}})_2]^{2-}$ , (*cis* or *trans*- $2^{\text{NN}}$ ), is  $\sim 3 \times 10^3$  kJ/mol higher in energy than the mono-deprotonated NO-chelation,  $\text{Cu}(\text{L}_{\text{mcpz}}\text{H})_2$ , (*cis* or *trans*- $2^{\text{NO}}$ ) precluding the existence of so far reported  $2^{\text{NN}}$  products. The calculations revealed that in all isomers, due to the mixing of  $d_{xy}^2$  orbital with a ligand group orbital as in **1**, 48–50% spin density is delocalized over the  $\text{L}_{\text{mcpz}}\text{H}_2$  ligand. In fluid solution, **1** absorbs strongly at 527 nm due to LMCT elucidated by the time dependent (TD) DFT calculations and the excited LMCT state is fluorescent ( $\lambda_{\text{ex}} = 375$  nm;  $\lambda_{\text{em}} = 405, 426$  nm;  $\Phi = 0.014$ ).

© 2016 Elsevier B.V. All rights reserved.

## 1. Introduction

Mono-hydrazone cuprizone ( $\text{L}_{\text{mcpz}}\text{H}_2$ ) is a bioactive molecule with neurotoxic properties leading to spongiosis and is used as a drug to induce that in laboratory animals [1–7]. Cuprizone has a strong affinity towards the redox active copper ion but the origin of the bioactivity of it is not clear so far [8–10]. To analyze the electronic and structural features mimicking the copper cuprizone complex, copper parent osazone ( $\text{PhNHN} = \text{CH} - \text{CH} = \text{NNHPh}$ ) complex was given attention. Reaction of osazone with copper(II) ion salt under argon in methanol affords a dark red precipitate which is unstable even in solid state and decomposes spontaneously at 298 K [11].

However, the reaction of benzil with 2-hydrazino pyridine in methanol in air yields a two electron paramagnetic dinuclear copper complex,  $(\text{CuLCl})_2$ , **1**, of  $(E)$ -1,2-diphenyl-2-(2-(pyridine-2-yl)hydrozono)ethanone (LH), an analogue of mono-hydrazone cuprizone ( $\text{L}_{\text{mcpz}}\text{H}_2$ ) as shown in Chart 1. A complete experimental and theoretical study substantiated the complex **1** which incorporates NNO chelate. To compare the ground state energies of the various chelation modes of cuprizone to copper(II) ion and the compositions of the molecular orbitals were analyzed by DFT

calculations. The calculations on the paramagnetic  $[\text{Cu}(\text{L}_{\text{mcpz}})_2]^{2-}$ , ( $2^{\text{NN}}$ ) or  $\text{Cu}(\text{L}_{\text{mcpz}}\text{H})_2$ , ( $2^{\text{NO}}$  or  $2^{\text{OO}}$ ) considering all three types of chelation as illustrated in Scheme 1, likewise, established that the frontier molecular orbitals of **1** are very similar to those of  $2^{\text{NN}}$ ,  $2^{\text{NO}}$  and  $2^{\text{OO}}$  analogues.

In this article, synthesis, structure, spectra and the unrestricted DFT calculations on **1**, *cis/trans* isomers of  $2^{\text{NO}}$ ,  $2^{\text{NN}}$  and  $2^{\text{OO}}$  are reported.

## 2. Experimental

## 2.1. Materials and physical measurements

Reagents or analytical grade materials were obtained from Sigma-Aldrich and used without further purification. Spectroscopic grade solvents were used for spectroscopic measurements. After evaporating  $\text{H}_2\text{O}$  and MeOH solvents of the sample under high vacuum, elemental analyses and spectral measurements were performed. The C, H and N content of the compounds were obtained from Perkin-Elmer 2400 series II elemental analyzer. Infrared spectra of the samples were measured from 4000 to 400  $\text{cm}^{-1}$  with the KBr pellet at 295 K on a Perkin-Elmer Spectrum RX 1, FT-IR Spectrophotometer. ESI mass spectra were recorded on a micro mass Q-TOF mass spectrometer. Electronic absorption spectra in solutions at 295 K were carried out on a Perkin-Elmer Lambda 25 spectrophotometer

\* Corresponding author.

E-mail address: [ghosh@pghosh.in](mailto:ghosh@pghosh.in) (P. Ghosh).

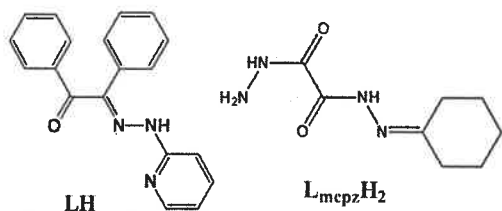


**Chart 1.** (E)-1,2-Diphenyl-2-(2-(pyridine-2-yl)hydrozono)ethanone (LH) and mono-hydrazone cuprizone ( $L_{mcpz}H_2$ ).

in the range of 1100–200 nm. Variable temperature (3–300 K) magnetization data were recorded in a 1 T magnetic field on a *SQUID magnetometer* (MPMS Quantum Design). The experimental magnetic susceptibility data were corrected for underlying magnetism using tabulated Pascal's constants and fit using *JulX* (Dr. Eckhard Bill). X-band EPR spectra were recorded on a *Bruker ELEXSYS E500* spectrometer and simulated with *XSophe* [12] distributed by Bruker Biospin GmbH. The electro analytical instrument, *BASI Epsilon-EC* for cyclic voltammetric experiments in  $CH_2Cl_2$  solutions containing 0.2 M tetrabutylammonium hexafluorophosphate as supporting electrolyte was used. The *BASI* platinum working electrode, platinum auxiliary electrode, *Ag/AgCl* reference electrode were used for the measurements.

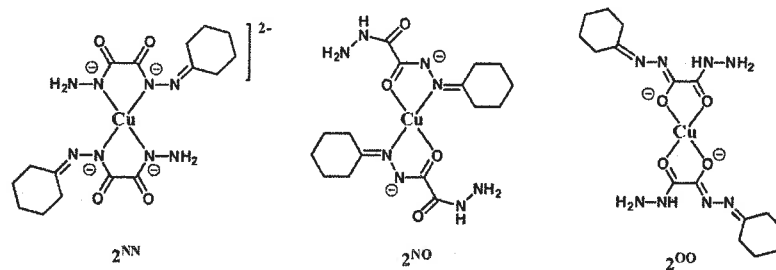
## 2.2. Syntheses

### 2.2.1. $[CuLCl]_2$ (1)

To a mixture of benzil (105 mg, 0.5 mmol) and 2-hydrazino pyridine (55 mg, 0.5 mmol) in a 100 mL round bottom flask, methanol (50 mL) was added and the reaction mixture was refluxed for 45 min (338 K). After cooling at room temperature (298 K), the solution mixture was filtered. To this solution anhydrous  $CuCl_2$  (70 mg, 0.5 mmol) in methanol (~10 mL) was added carefully and the reaction mixture was allowed to evaporate slowly at 298 K. After a few days, a green crystalline solid of **1** separated out, which were filtered and dried in air and collected. Yield: 96 mg (~51% with respect to copper). Mass spectrum (ESI, positive ion,  $CH_3CN$ );  $m/z$ : 363 for ( $CuL^+$ ). Anal. Calc. for  $C_{38}H_{28}Cl_2Cu_2N_6O_2$ : C, 57.15; H, 3.53; N, 10.52; Found: C, 57.25; H, 3.55; N, 10.45. IR (KBr disk):  $\nu$  3474 (s), 1602 (vs), 1456 (m), 1514 (m), 1466 (s), 1438 (s), 1358 (s), 1327 (s), 1208 (vs), 1141 (s), 1092 (s), 1012 (s), 927 (m), 778 (m), 702 (s), 665 (vs)  $cm^{-1}$ .

### 2.3. Structure determination

Single crystals of **1** was picked up with nylon loops and was mounted on a *Bruker APEX-II CCD* diffractometer equipped with a Mo-target rotating-anode X-ray source and a graphite monochromator (Mo- $K\alpha$ ,  $\lambda = 0.71073$  Å). Final cell constants were obtained from least squares fits of all measured reflections.



**Scheme 1.** Possible chelation modes of  $L_{mcpz}H_2$ :  $[Cu(L_{mcpz}H_2)]^{2-}$  ( $2^{NN}$ ) and  $[Cu(L_{mcpz}H_2)]$  ( $2^{NO}$  and  $2^{OO}$ ).

**Table 1**  
Crystallographic data for **1**.

CCDC	840632	$\rho_c/g\text{ cm}^{-3}$	1.525
Formula	$C_{38}H_{28}Cl_2Cu_2N_6O_2$	$2\theta_{max}$	50.0
$F_w$	798.64	Unique reflections	8375
Crystal colour	Green	Total reflections	12939
Crystal system	Monoclinic	$\lambda/\text{Å}$	0.71073
Space group	$C2/c$	$\mu/\text{mm}^{-1}$	1.421
$a/\text{Å}$	21.9360(5)	$F(0\ 0\ 0)$	1624
$b/\text{Å}$	9.8104(2)	$R_1^a$ [ $>2\sigma(I)$ ]	0.0257
$c/\text{Å}$	17.5925(4)	GOF <sup>b</sup>	1.02
$\beta/^\circ$	113.27(1)	$R_1^c$ (all data)	0.0297
$V/\text{Å}^3$	3477.87(13)	$wR_2^c$ [ $>2\sigma(I)$ ]	0.0743
Z	4	No. of Parameter	226
$T/K$	296(2)	$\Delta\rho_{max,min}/e\text{Å}^{-3}$	0.508/−0.348

Observation criterion:  $I > 2\sigma(I)$ .

<sup>a</sup>  $R_1 = \sum ||F_o| - |F_c|| / \sum |F_o|$ .

<sup>b</sup>  $GOF = \{ \sum [w(F_o^2 - F_c^2)^2] / (n - p) \}^{1/2}$ .

<sup>c</sup>  $wR_2 = \{ \sum [w(F_o^2 - F_c^2)^2] / \sum [w(F_o^2)^2] \}^{1/2}$  where  $w = 1 / [\sigma^2(F_o^2) + (aP)^2 + bP]$ .

$P = (F_o^2 + 2F_c^2) / 3$ .

Intensity data were corrected for absorption using intensities of redundant reflections. The structure was readily solved by direct methods and subsequent difference Fourier techniques. The crystallographic data of **1** are listed in Table 1. The *Siemens SHELXS97* [13] software package was used for solution and *SHELXL97* [13] was used for the refinement. All non-hydrogen atoms were refined anisotropically. Hydrogen atoms were placed at the calculated positions and refined as riding atoms with isotropic displacement parameters.

### 2.4. Density functional theory (DFT) calculations

All calculations reported in this chapter were done with the *Gaussian 03W* [14] program package supported by *GaussView 4.1*. The DFT [15] and TD DFT [16] calculations were performed at the level of Becke three parameter hybrid functional with the non-local correlation functional of Lee-Yang-Parr (B3LYP) [17]. The gas phase geometries of **1**,  $t\text{-}2^{NO}$ ,  $c\text{-}2^{NO}$ ,  $t\text{-}2^{NN}$ ,  $c\text{-}2^{NN}$  and  $2^{OO}$  were optimized on theoretical coordinates using Pulay's Direct Inversion [18] in the Iterative Subspace (DIIS) convergent SCF procedure [19] ignoring symmetry. In all calculations, a LANL2DZ basis set along with the corresponding effective core potential (ECP) was used for copper metal [20]. Valence double zeta basis set, 6-31G [21] for H was used. For C, N, O and Cl non-hydrogen atoms valence double zeta plus diffuse and polarization functions, 6-31G (d,p) [22] as basis set were employed for the calculations. The percentage contribution of ligand and metal to the frontier orbitals of **1** and  $t\text{-}2^{NO}$  were calculated using *GaussSum* program package [23]. The sixty lowest singlet excitation energies on the optimized geometries of **1** in  $CH_2Cl_2$  using CPCM model [24] were elucidated by TD DFT method.

### 3. Results and discussion

#### 3.1. Syntheses and characterization

The tridentate NNO-donor chelating agent, (*E*)-1,2-diphenyl-2-(2-(pyridine-2-yl)hydrazono)ethanone (LH), was not pre-isolated. The reaction of benzyl and 2-hydrazinopyridine with anhydrous  $\text{CuCl}_2$  in methanol affords **1** in a moderate yield (~51% with respect to copper). The composition of **1** was substantiated by mass, IR spectra and elemental analyses including the single crystal X-ray structure determination. Like copper-cuprizonone complex with a lower energy absorption band at 609 nm [8], **1** absorbs strongly at 527 nm. The electronic spectrum of **1** is shown in Fig. 1a and the spectral parameters are summarized in Table 2. TD DFT calculations elucidated the origins of such transitions (*vide infra*). The  $\text{CH}_2\text{Cl}_2$  solution of **1** is fluorescent at 295 K. The structured excitation and emission spectra are illustrated in Fig. 1b and emission

parameters are summarized in Table 2. The quantum yield was calculated with respect to anthracene.

#### 3.2. X-ray structure of **1**

Single crystal X-ray structure determination confirmed the molecular geometry of **1** in crystals. It crystallizes in space group  $C2/c$ . The molecular structure with the atom numbering scheme is depicted in Fig. 2 and the relevant bond parameters are summarized in Table 3. In **1**, two  $\text{CuCl}_2\text{N}_2\text{O}$  coordination spheres with distorted trigonal bipyramid (tbp) geometries are equivalent.

$\text{Cu}(1)$ ,  $\text{Cl}(1)$ ,  $\text{Cl}(1A)$  and  $\text{N}(3)$  sites are on the equatorial plane with mean deviation 0.005 Å while  $\text{O}(1)$ ,  $\text{Cu}(1)$  and  $\text{N}(1)$  atoms make the axial bond with  $158.91(6)^\circ$ . The tridentate chelate with the pyridine ring is planar (mean deviation 0.04 Å). The orientations of the two pendant phenyl rings of the benzil fragment are different and respectively at dihedral angles of  $24^\circ$  and  $66^\circ$  to the

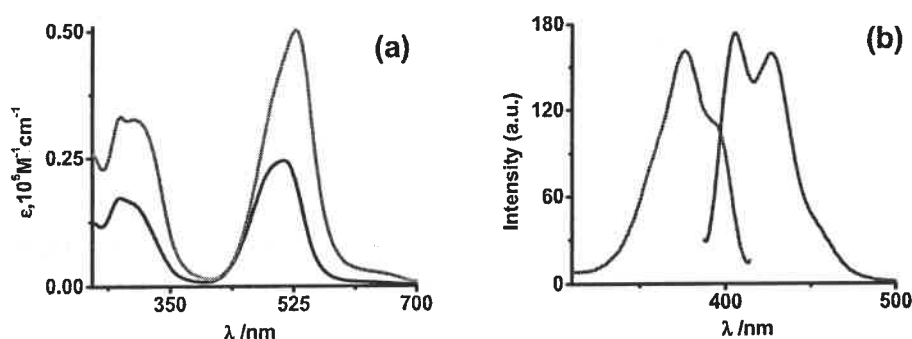


Fig. 1. (a) Electronic spectra in  $\text{CH}_2\text{Cl}_2$  (red) and  $\text{CH}_3\text{CN}$  (black) and (b) excitation (green) and emission (violet) spectra in  $\text{CH}_2\text{Cl}_2$  of **1** at 295 K. (For interpretation of the references to colour in this figure legend, the reader is referred to the web version of this article.)

Table 2  
Electronic and fluorescence spectral data of **1** in  $\text{CH}_2\text{Cl}_2$  and  $\text{CH}_3\text{CN}$  at 295 K.

Solvent	UV-vis spectral data $\lambda_{\text{max}}$ nm ( $\epsilon$ , $10^5 \text{ M}^{-1} \text{ cm}^{-1}$ )	Fluorescence spectral data
$\text{CH}_2\text{Cl}_2$	527 (0.49), 301 (0.32), 280 (0.33)	$\lambda_{\text{ex}} = 375 \text{ nm}$ ; $\lambda_{\text{em}} = 405, 426 \text{ nm}$ ; $\Phi = 0.014$
$\text{CH}_3\text{CN}$	510 (0.25), 299 (0.16), 278 (0.17)	Non-emissive

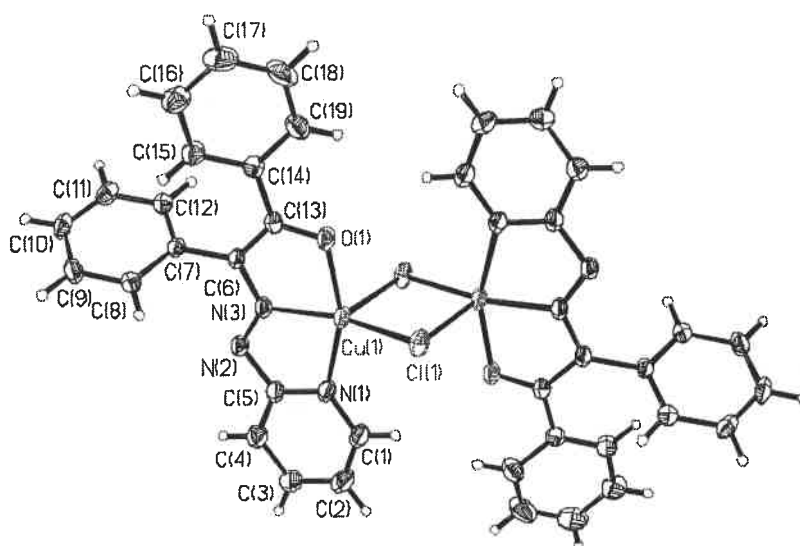


Fig. 2. Molecular structure of **1** in crystals.

**Table 3**  
Selected experimental and calculated bond distances (Å) and angles (deg) of **1**.

	Experimental	Calculated
Cu(1)–N(1)	1.9896(17)	2.0491
Cu(1)–N(3)	1.9392(14)	2.0099
Cu(1)–O(1)	1.9922(14)	2.0342
Cu(1)–Cl(1)	2.2553(5)	2.3079
N(3)–N(2)	1.306(2)	1.2949
N(3)–C(6)	1.335(2)	1.3407
N(1)–C(5)	1.357(2)	1.3618
N(2)–C(5)	1.389(2)	1.3843
O(1)–C(13)	1.267(2)	1.2717
C(6)–C(13)	1.442(2)	1.4511
N(3)–Cu(1)–N(1)	79.07(6)	77.67
N(3)–Cu(1)–O(1)	80.34(6)	79.12
N(1)–Cu(1)–Cl(1)	100.20(5)	99.96
O(1)–Cu(1)–Cl(1)	97.37(4)	95.37
Cl(1)–Cu(1)–Cl(1)	92.921(18)	93.04

tridentate chelate. The Cl(1)–Cu(1)–Cl(1A) angle, 92.9°, is much shorter than ideal 120° for a *tbp* geometry. The C(13)–O(1) length, 1.267(2) Å, is consistent to the C=O double bond. The negative charge of the ligand is primarily localized on the [N(2)–N(3)=C(6) ↔ N(2)=N(3)–C(6)] fragment having comparatively shorter N(2)–N(3) 1.306(2) Å (longer than –N=N– length) and longer N(3)–C(6) 1.335(2) Å (shorter than a N–C length) distances. The C(13)–C(6) length, 1.442(2) Å, is comparable to a C<sub>sp</sub>–C<sub>sp</sub> single bond length. The non-bonding Cu(1)–Cu(1A) distance is 3.348 Å. The Cu(1)–Cl(1), Cu(1)–N(3) and Cu(1)–N(1) distances in **1** are relatively shorter than those reported in similar type of Cu(II) complexes [25].

### 3.3. Magnetic susceptibility and the EPR spectroscopy

The temperature dependence of the magnetic susceptibility of **1** was studied at 3–300 K using a SQUID magnetometer (1 T external field). A temperature independent effective magnetic moment of 2.58 μ<sub>B</sub> was observed above 30 K (Fig. 3). The data were modelled using the isotropic exchange Hamiltonian,  $\hat{H}_{ex} = -2JS_1S_2$ , where  $J$  is the isotropic exchange coupling constant and  $S_1 = S_2 = 1/2$  for each Cu(II) d<sup>9</sup> ion. The best fit was obtained with a minute exchange coupling of  $J = -1.0(1) \text{ cm}^{-1}$  (for  $g = 2.112$ ) in **1** indicates the Cu(II) ions are very weakly coupled by virtue of their co-planarity. This very small exchange coupling precludes assignment of the total spin ground state in **1**, and therefore,  $J$  should

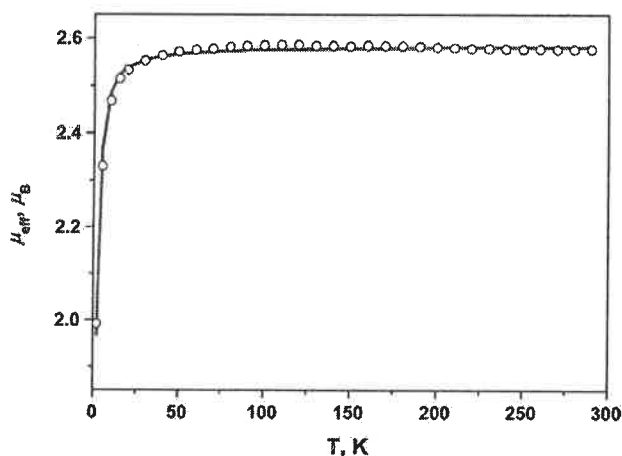


**Fig. 3.** Temperature dependence of the magnetic moment,  $\mu_{\text{eff}}/\mu_{\text{B}}$ , of powdered sample of **1**. The circles represent the experimental data, whereas the solid lines represent simulations (see text).

be treated as an absolute value. The near degenerate singlet–triplet ground state in **1** makes it amenable to interrogation by EPR spectroscopy.

The EPR signal of the allowed transitions ( $\Delta M_s = 1$ ) was significantly broadened, however we observe a rather striking seven-line feature at half-field (160 mT) signal due to the forbidden “ $\Delta M_s = 2$ ” transition of the triplet state generated by the weakly coupled Cu(II) ions in **1**. Experimental and simulated X-band EPR spectra were depicted in Fig. 4. The seminal work of Pilbrow and coworkers established the guidelines for interpreting such half-field signals [26] and we simulated the spectrum using  $g$ ,  $A$ ,  $J$ , and the inter-atomic Cu···Cu distance,  $r = 3.35 \text{ Å}$  as determined by X-ray crystallography (*vide supra*). The simulation gave  $g = (2.121, 2.005, 2.004)$  and  $A = (171, 13, 13) \times 10^{-4} \text{ cm}^{-1}$  for each Cu(II) ion, the line-shape and overall position was greatly improved by including an Euler angle,  $\xi = 31^\circ$ , that is defined as the angle between the inter-atomic Cu···Cu vector and the “z-axis” of the first site, though the exact reference to the coordinate frame was not known. With the extreme broadening of the allowed transitions for **1**, we are unable to unambiguously vet the principle  $g$  and  $A$ -values, the mean  $g$ -value,  $\langle g \rangle = 2.043$  is in good agreement with the one derived from the magnetic data,  $g = 2.112$ . The  $J$ -value was fixed from the magnetic susceptibility fit as in this regime with  $J$  comparable to the microwave energy ( $0.3 \text{ cm}^{-1}$  at X-band), the half-field signal is relatively insensitive to the precise value. On the whole, this spectrum is clearly diagnostic of two weakly coupled Cu(II) d<sup>9</sup> ions with a  $d_{xy}^2$  SOMO.

### 3.4. Electronic structures

The electronic structures of **1** and copper-cuprizonate system were elucidated by unrestricted density functional theory (DFT) calculations on **1**, and *cis/trans* isomers of **2<sup>NO</sup>**, **2<sup>NN</sup>** and **2<sup>OO</sup>**. The gas phase geometry of **1** was optimized by unrestricted DFT calculations respectively with triplet ( $S = 1$ ) and doublet ( $S = 1/2$ ) spin

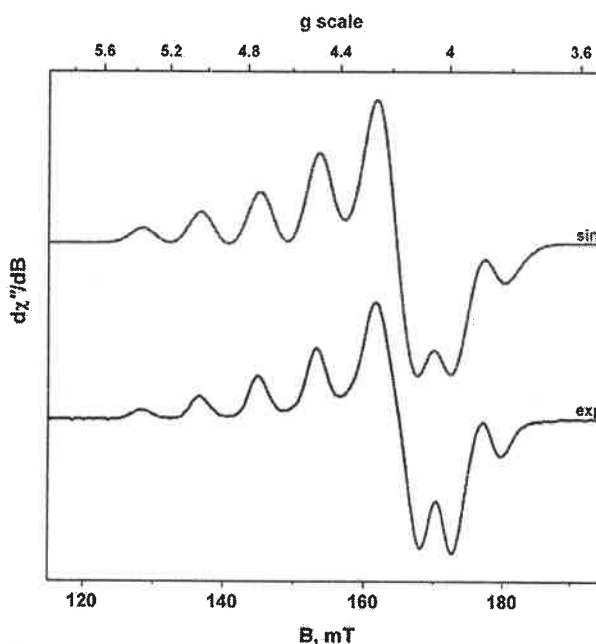


**Fig. 4.** X-band EPR spectrum of **1** at half-field recorded in CH<sub>2</sub>Cl<sub>2</sub>/toluene at 10 K. Experimental spectrum shown in black, simulation depicted in red (conditions: frequency 9.632 GHz; power 20 mW; modulation 0.7 mT). (For interpretation of the references to colour in this figure legend, the reader is referred to the web version of this article.)

states. Calculated bond parameters summarized in Table 3 are very similar to those observed experimentally in **1**. Structures of two SOMOs of **1** are illustrated in Fig. 5a. Both the SOMOs are composed of 48%  $d_{xy}^2$  (Cu) + 52% ligand. Mulliken spin population analyses have established the following alpha spin distribution in **1**: Cu, 0.50; N1, 0.20; N2, 0.18; O, 0.19. The spin density distribution is illustrated in Fig. 5b. The calculations therefore conclude that the binding of  $L^-$  to the Cu(II) ion results a strong  $\sigma$ -interaction with the  $d_{xy}^2$  orbital and the unpaired electron resides on  $\sigma^*$  orbital which is composed of  $d_{xy}^2$  and a ligand group orbital.

The important outcome of these calculations was that the energies of  $\pi_{\text{imine}^*}$  orbitals of **1** as illustrated in Fig. 6 are higher (alpha  $\pi^*$  orbital  $\sim 362$  kJ/mol and beta orbital  $\sim 48$  kJ/mol) than the corresponding  $\sigma$ -antibonding orbitals those are composed of  $d_{xy}^2$  and a ligand group orbitals.

In all cases, the SOMO is the  $\sigma$ -antibonding orbital composed of  $d_{xy}^2$  and ligand and likewise the spin density is distributed over the copper ion ( $\sim 50\%$ ) and ligand ( $\sim 50\%$ ). Shifting of spin density to the

ligand by this type of interaction makes the Cu(II) to Cu(III) transformation easier, which has enormous effect on structures and reactivities of these species. The experimental observations are: (a) all these species tend to have square-planar geometry, the most favourable geometry of a  $d^8$  ion and (b) these species are reactive and unstable in solutions. All these features can be explained well by the formation of reactive Cu(III), a  $d^8$  ion which is observed in copper-cuprizon chemistry [8–10].

### 3.5. Occupied and unoccupied photoactive molecular orbitals (OPMO and UPMOs)

The electronic spectral features of copper cuprizon complex and **1** are very similar. Both species exhibit lower energy absorption bands above 500 nm. The origins of these bands were elucidated by TD DFT calculation on **1**. Sixty lowest singlet excitation energies on the optimized geometries were calculated in  $\text{CH}_2\text{Cl}_2$  using conductor-like polarisable continuum (CPCM) model.

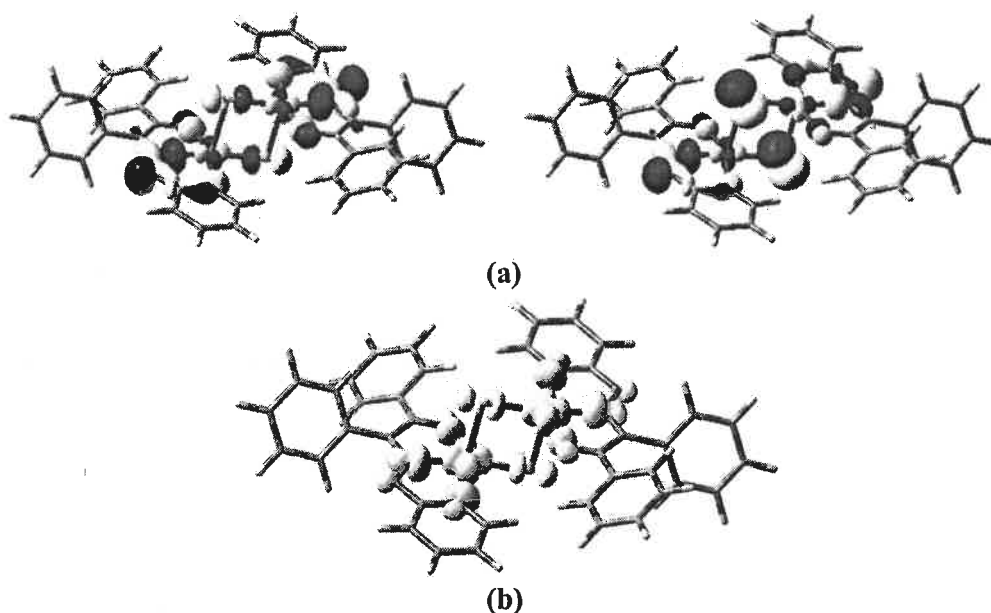


Fig. 5. (a) Two SOMOs and (b) Mulliken spin density plot of **1**.

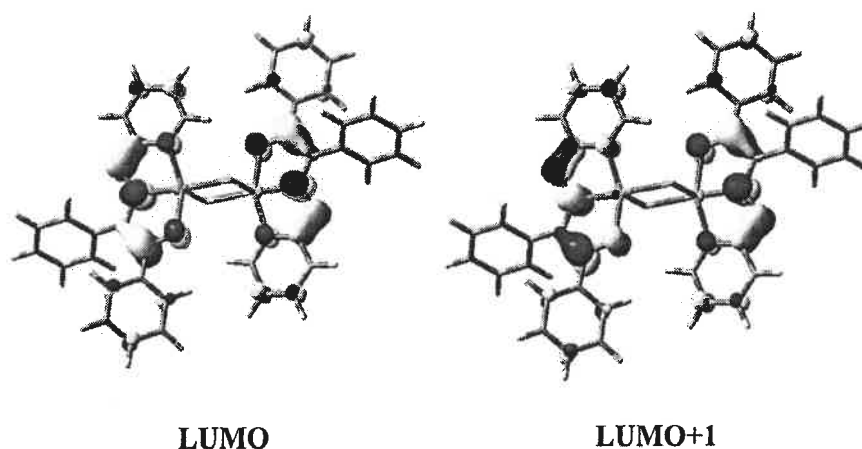


Fig. 6. Unoccupied alpha  $\pi^*$  orbitals of **1**.

Table 4

Excitation energies ( $\lambda/\text{nm}$ ), oscillator strengths ( $f$ ), transition types and dominant contributions of UV-vis absorption bands of **1** in  $\text{CH}_2\text{Cl}_2$  obtained from TD DFT calculations.

$\lambda_{\text{cal}}$ (nm)	$f$	$\lambda_{\text{exp}}$ (nm)	Significant Transitions (>15%)	Dominant type
519	0.015	527	$\beta$ OCMOs <sup>b</sup> $\rightarrow$ LUMO (90)	$L \rightarrow (d_{xy}^2-L)^a$
507	0.388		$\alpha$ HOMO-1 $\rightarrow$ LUMO (22)	$(d_{xy}^2+L) \rightarrow L$
			$\alpha$ HOMO $\rightarrow$ LUMO (25)	$L \rightarrow L$
			$\beta$ HOMO-1 $\rightarrow$ LUMO+1 (26)	$L \rightarrow L$
482	0.142		$\alpha$ HOMO-1 $\rightarrow$ LUMO (62)	$L \rightarrow L$
445	0.025		$\beta$ HOMO-1 $\rightarrow$ LUMO (75)	$L \rightarrow (d_{xy}^2-L)^a$
436	0.035		$\beta$ HOMO-2 $\rightarrow$ LUMO (69)	$L \rightarrow (d_{xy}^2-L)^a$
414	0.073		$\beta$ HOMO-7 $\rightarrow$ LUMO (29)	$(L+d_{xy}^2) \rightarrow (d_{xy}^2-L)^a$
			$\beta$ HOMO-6 $\rightarrow$ LUMO (30)	$(L+d_{xy}^2) \rightarrow (d_{xy}^2-L)^a$
404.2	0.036		$\beta$ HOMO-3 $\rightarrow$ LUMO (64)	$L \rightarrow (d_{xy}^2-L)^a$
377.8	0.027		$\beta$ HOMO-9 $\rightarrow$ LUMO (17)	$L \rightarrow (d_{xy}^2-L)^a$
			$\beta$ HOMO-8 $\rightarrow$ LUMO (25)	$L \rightarrow (d_{xy}^2-L)^a$

<sup>a</sup> Minus(-) sign designate antibonding orbital.

<sup>b</sup> OCMOs = occupied molecular orbitals of ligand.

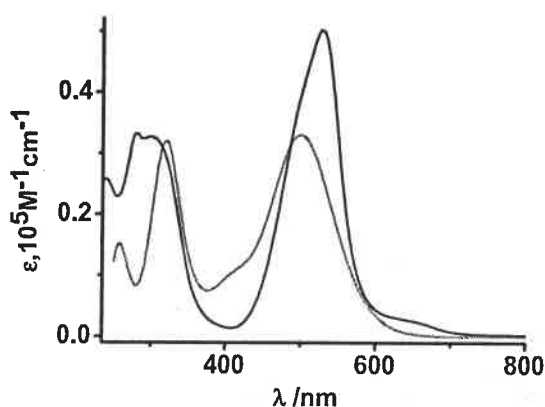


Fig. 7. Experimental (black) and calculated (red) electronic absorption spectra (obtained from TD DFT calculations) of **1** in  $\text{CH}_2\text{Cl}_2$ . (For interpretation of the references to colour in this figure legend, the reader is referred to the web version of this article.)

Calculated energies, dominant contributions, and transition types of these calculations were listed in Table 4. The calculated spectrum that correlates well to the experimental spectrum recorded in  $\text{CH}_2\text{Cl}_2$  is illustrated in Fig. 7. The calculations thus authenticated that the characteristic lower energy absorption is due to the transitions to the unoccupied  $\beta$ -LUMO, and the  $\beta$ -SOMO.

### 3.6. Electron transfer events (ETEs)

The electron transfer events of **1** in  $\text{CH}_2\text{Cl}_2$  solution under completely  $\text{N}_2$  atmosphere were studied by cyclic voltammetry. The experiments predict that all the electron transferred products of **1** are unstable and ETEs are solvent dependent. In  $\text{CH}_2\text{Cl}_2$  solvent, one of the irreversible ETEs that occur at  $-0.8$  V with respect to  $\text{Fc}^+/\text{Fc}$  couple as shown in Fig. 8 are recorded very quickly in different scan rates. The cathodic peak was assigned to the reduction of **1** to **1**<sup>-</sup> and electron goes to the SOMO that is composed of metal  $d_{xy}^2$  and a ligand orbital.

### 3.7. Molecular and electronic structures of isomeric copper-cuprizonone complexes (cis/trans-2<sup>NO</sup>, 2<sup>NN</sup> and 2<sup>OO</sup>)

In the context of this research, the molecular and electronic structures of copper cuprizonone complex were investigated by spin unrestricted DFT calculations. The calculated stable molecular

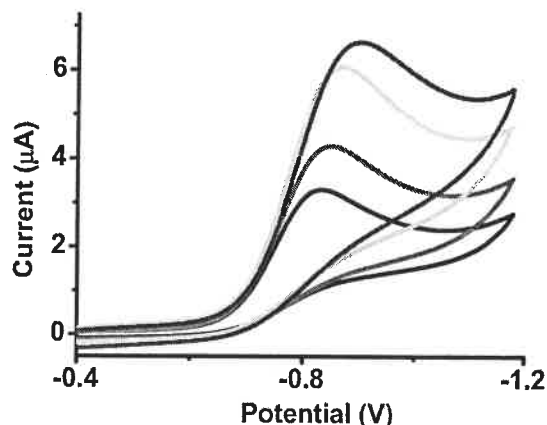
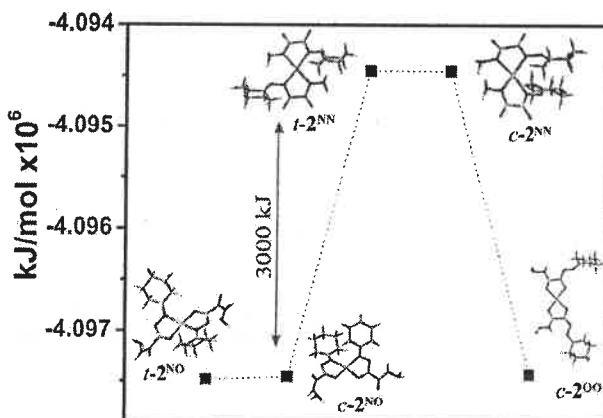


Fig. 8. Cyclic voltammograms of **1** in  $\text{CH}_2\text{Cl}_2$  at 295 K. Conditions: 0.2 M  $[\text{N}(n\text{-Bu})_4]\text{PF}_6$  supporting electrolyte; scan rates 50 (black), 100 (green) and 400 (blue)  $\text{mV s}^{-1}$ ; platinum working electrode. (For interpretation of the references to colour in this figure legend, the reader is referred to the web version of this article.)



Scheme 2. Relative ground state energies of isomeric copper cuprizonone complexes (gas phase).

geometry contradicts the existence of reported NN-coordinated copper cuprizonone complex. It is unambiguously proved by Messori et al. [8] and Nilsson [1] that mono-hydrazone ( $\text{L}_{\text{mcpz}}\text{H}_2$ , Chart 1) rather than a di-hydrazone actually chelates the  $\text{Cu}(\text{II})$  ion. The question is whether  $\text{L}_{\text{mcpz}}\text{H}_2$  undergoes mono-deprotonation ( $\text{L}_{\text{mcpz}}\text{H}^-$ ) or bis-deprotonation ( $\text{L}_{\text{mcpz}}^{2-}$ ), the second process particularly needs removal of a proton from the unfavourable basic  $-\text{NHNH}_2$  unit. The dominant peak at  $m/z = 457$  in the ESI (positive ion) mass spectrum reported by Messori et al. [8] is consistent with the presence of only mono-deprotonated ( $\text{L}_{\text{mcpz}}\text{H}^-$ ) mono-hydrazone cuprizonone derivative producing neutral  $\text{Cu}^{\text{II}}(\text{L}_{\text{mcpz}}\text{H})_2$  or cationic  $[\text{Cu}^{\text{III}}(\text{L}_{\text{mcpz}}\text{H})_2]^+$  products. Chelation of bis-deprotonated ( $\text{L}_{\text{mcpz}}^{2-}$ ) cuprizonone derivative affords only anionic product,  $[\text{Cu}^{\text{III}}(\text{L}_{\text{mcpz}}^{2-})_2]^-$  that is detectable in ESI (negative ion) mass spectrum. Further the presence of strong band at  $3160 \text{ cm}^{-1}$  in FT IR spectrum does not support the presence of bis-deprotonated derivative. To respond all these features of IR and ESI mass spectra, all the possible isomeric geometries (cis/trans-2<sup>NN</sup>, 2<sup>NO</sup> and 2<sup>OO</sup>; Scheme 1) of the copper cuprizonone systems in gas phase were optimized for comparison.

Surprisingly, it is observed that the ground state energy of **t-2<sup>NN</sup>** (Scheme 1; reported NN-coordinated trans-geometry incorporating bis-deprotonated mono-hydrazone cuprizonone) or **c-2<sup>NN</sup>** (NN-coordinated cis-geometry incorporating bis-deprotonated mono-hydrazone cuprizonone) is  $\sim 3 \times 10^3$  kJ/mol higher than the



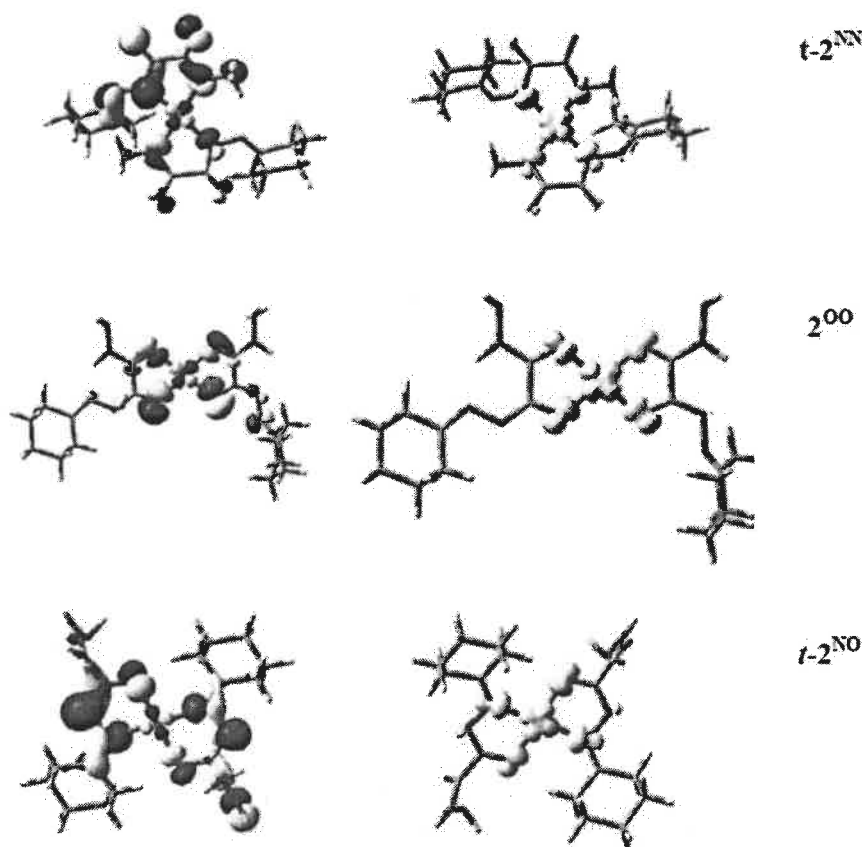


Fig. 9. Structures of SOMOs and Mulliken spin density plots of (a)  $t-2^{NN}$ , (b)  $t-2^{NO}$  and (c)  $2^{OO}$ .

most stable alike 1 keto-imine binding,  $t-2^{NO}$  (NO-coordinated *trans*-geometry incorporating mono-deprotonated mono-hydrazone cuprizone like 1), while the  $2^{OO}$  (OO-coordinated mono-deprotonated mono-hydrazone cuprizone) is only  $\sim 30$  kJ/mole higher in energy than  $t-2^{NO}$  or  $c-2^{NO}$  (Scheme 1). A diagram to compare the energies of the isomers is illustrated in Scheme 2. The study forbids the existence of  $t-2^{NN}$  or  $c-2^{NN}$  those were considered so far as the most stable binding mode of cuprizone to copper ion.

Analyses of molecular orbitals and atomic spin densities established the electronic structures of  $t-2^{NN}$ ,  $c-2^{NN}$ ,  $t-2^{NO}$ ,  $c-2^{NO}$  and  $2^{OO}$  complexes. In all cases, similar to 1, SOMO is an antibonding orbital constituted of  $d_{Cu}$  (48–51%) and a ligand group orbital (52–49%) as illustrated in the Fig. 9. The spin density thus is delocalized over the copper (48–51%) as well as on the coordinated N and O donor centers of the ligand (Fig. 9). The feature defines the cuprizone as strong  $\sigma$ -donor agent. It facilitates the ease removal of the electrons from the cuprizone complexes and augments the formation of diamagnetic Cu(III)-cuprizone complexes in air [8–10]. The study thus proclaims that coordination of cuprizone to the biologically available copper(II) ion irrespective of the binding mode results stronger reducing equivalent initiating the formation of reactive chemical species like superoxide/peroxide and copper (III) ion which are important sources of the toxic effects of cuprizone to the living systems.

#### 4. Conclusion

An analogue of copper cuprizone complex,  $[CuLCl]_2$  (1), with (*E*)-1,2-diphenyl-2-(2-(pyridine-2-yl)hydrozono)ethanone (LH),

was isolated and substantiated by spectra, single crystal X-ray structure, *SQUID* measurement and unrestricted DFT calculations. The EPR spectroscopy predicts the existence of two weakly coupled Cu(II)  $d^9$  ions in 1. Electronic structural and spectral features of 1 and copper cuprizone analogues are similar. DFT calculations on all the possible isomeric copper chelates of cuprizone authenticated that mono-deprotonated NO-chelates of mono-hydrazone cuprizone derivative alike 1 affording  $Cu(L_{mcpz}H)_2$ , (*cis* or *trans*- $2^{NO}$ ) have the minimum ground state energy, while the *bis*-deprotonated NN-chelates,  $[Cu(L_{mcpz})_2]^{2-}$ , (*cis* or *trans*- $2^{NN}$ ), are  $\sim 3 \times 10^3$  kJ/mol higher in energy than the corresponding NO-chelates. This result contradicts the formation or existence of so far reported NN-chelated copper cuprizone complex. Molecular orbital analyses revealed that the mixing of  $d_{xy}^2$  orbital with a ligand group  $\sigma$  orbital of 1 and copper cuprizone shifts 48–50% spin density to the corresponding ligand backbone that make these species reducing agent in the living system.

#### Acknowledgments

Financial support received from DST (SR/S1/IC/0026/2012) and CSIR (01/2699/12/EMR-II), New Delhi, India is gratefully acknowledged. S.K. is thankful to CSIR, New Delhi, India, for SRF fellowships.

#### Appendix A. Supplementary data

Supplementary data associated with this article can be found, in the online version, at <http://dx.doi.org/10.1016/j.ica.2016.06.040>.

## References

- [1] (a) G. Nilsson, *Anal. Chem.* 153 (1956) 161;  
(b) G. Nilsson, *Acta Chem. Scand.* 4 (1950) 250.
- [2] P. Zatta, M. Raso, P. Zambenedetti, W. Wittkowski, L. Messori, F. Piccioli, P.L. Mauri, M. Beltramini, *Cell. Mol. Life Sci.* 62 (2005) 1502.
- [3] (a) G.R. Clark, B.W. Skelton, T.N. Waters, *J. Chem. Soc. Dalton Trans.* (1976) 1528;  
(b) G.R. Clark, B.W. Skelton, T.N. Waters, *J. Chem. Soc. Chem. Commun.* (1972) 1163.
- [4] J. Oliver, T.N. Waters, *J. Chem. Soc. Chem. Commun.* (1982) 1111.
- [5] W.E. Keyes, J.B.R. Dunn, T.M. Loefer, *J. Am. Chem. Soc.* 99 (1977) 4527.
- [6] (a) I.O. Fritsky, H. Kozłowski, O.M. Kanderai, M. Haukka, J.S. Kozłowska, E.G. Kontecka, F. Meyer, *Chem. Commun.* (2006) 4125;  
(b) I.O. Fritsky, H. Kozłowski, P.J. Sadler, O.P. Yefetova, J.S. Kozłowska, V.A. Kalibabchuk, T. Glowiak, *J. Chem. Soc. Dalton Trans.* (1998) 3269.
- [7] (a) I.H. Pattison, J.N. Jebbett, *Res. Vet. Sci.* 14 (1973) 128;  
(b) I.H. Pattison, J.N. Jebbett, *J. Pathol.* 109 (1973) 245;  
(c) I.H. Pattison, J.N. Jebbett, *Nature* 230 (1971) 115;  
(d) I.H. Pattison, J.N. Jebbett, *Res. Vet. Sci.* 12 (1971) 378.
- [8] L. Messori, A. Casini, C. Gabbiani, L. Sorace, M.M. Miranda, P. Zatta, *Dalton Trans.* (2007) 2112.
- [9] M.M. Miranda, M. Pagliai, G. Cardini, L. Messori, B. Bruni, A. Casini, M. Di Vaira, V. Schettino, *Cryst. Eng. Commun.* 10 (2008) 416.
- [10] N. Yamamoto, K. Kuwata, *J. Mol. Struct.* 52 (2009) 52.
- [11] (a) S.C. Patra, M.K. Biswas, A.N. Maity, P. Ghosh, *Inorg. Chem.* 50 (2011) 1331;  
(b) A.S. Roy, H.M. Tuononen, S.P. Rath, P. Ghosh, *Inorg. Chem.* 46 (2007) 5942.
- [12] G.R. Hanson, K.E. Gates, C.J. Noble, M. Griffin, A. Mitchell, S. Benson, *J. Inorg. Biochem.* 98 (2004) 903.
- [13] (a) G.M. Sheldrick, ShelX597, Universität Göttingen, Göttingen, Germany, 1997;  
(b) G.M. Sheldrick, ShelXL97, Universität Göttingen, Göttingen, Germany, 1997.
- [14] M.J. Frisch, G.W. Trucks, H.B. Schlegel, G.E. Scuseria, M.A. Robb, J.R. Cheeseman Jr., J.A. Montgomery, T. Vreven, K.N. Kudin, J.C. Burant, J.M. Millam, S.S. Iyengar, J. Tomasi, V. Barone, B. Mennucci, M. Cossi, G. Scalmani, N. Rega, G.A. Petersson, H. Nakatsuji, M. Hada, M. Ehara, K. Toyota, R. Fukuda, J. Hasegawa, M. Ishida, T. Nakajima, Y. Honda, O. Kitao, H. Nakai, M. Klene, X. Li, J.E. Knox, H. P. Hratchian, J.B. Cross, V. Bakken, C. Adamo, J. Jaramillo, R. Gomperts, R.E. Stratmann, O. Yazyev, J.A. Austin, R. Cammi, C. Pomelli, J.W. Ochterski, P.Y. Ayala, K. Morokuma, G.A. Voth, P. Salvador, J.J. Dannenberg, V.G. Zakrzewski, S. Dapprich, A.D. Daniels, M.C. Strain, O. Farkas, D.K. Malick, A.D. Rabuck, K. Raghavachari, J.B. Foresman, J.V. Ortiz, Q. Cui, A.G. Baboul, S. Clifford, J. Cioslowski, B.B. Stefanov, G. Liu, A. Liashenko, P. Piskorz, I. Komaromi, R.L. Martin, D.J. Fox, T. Keith, M.A. Al-Laham, C.Y. Peng, A. Nanayakkara, M. Challacombe, P.M.W. Gill, B. Johnson, W. Chen, M.W. Wong, C. Gonzalez, J.A. Pople, *Gaussian 03. Revision E.01*, Gaussian, Inc., Wallingford, CT, 2004.
- [15] (a) R.G. Parr, W. Yang, *Density Functional Theory of Atoms and Molecules*, Oxford University Press, Oxford, UK, 1989;  
(b) D.R. Salahub, M.C. Zerner, *The Challenge of D and F Electrons*; ACS Symposium Series 394, American Chemical Society, Washington, DC, 1989;  
(c) W. Kohn, L. Sham, *J. Phys. Rev.* 104 (1965) A1133;  
(d) P. Hohenberg, W. Kohn, *Phys. Rev.* 136 (1964) B864.
- [16] (a) R.E. Stratmann, G.E. Scuseria, M. Frisch, *J. Chem. Phys.* 109 (1998) 8218;  
(b) M.E. Casida, C. Jamoroski, K.C. Casida, D.R. Salahub, *J. Chem. Phys.* 108 (1998) 4439;  
(c) R. Bauernschmitt, M. Haser, O. Treutler, R. Ahlrichs, *Chem. Phys. Lett.* 256 (1996) 454.
- [17] (a) A.D. Becke, *J. Chem. Phys.* 98 (1993) 5648;  
(b) B. Miehlich, A. Savin, H. Stoll, H. Preuss, *Chem. Phys. Lett.* 157 (1989) 200;  
(c) C. Lee, W. Yang, R.G. Parr, *Phys. Rev. B* 37 (1988) 785.
- [18] P.J. Pulay, *Comput. Chem.* 3 (1982) 556.
- [19] H.B. Schlegel, J.J. McDouall, in: C. Ogretir, I.G. Csizmadia (Eds.), *Computational Advances in Organic Chemistry*, Kluwer Academic, The Netherlands, 1991, pp. 167–185.
- [20] (a) P.J. Hay, W.R. Wadt, *J. Chem. Phys.* 82 (1985) 270;  
(b) W.R. Wadt, P.J. Hay, *J. Chem. Phys.* 82 (1985) 284;  
(c) P.J. Hay, W.R. Wadt, *J. Chem. Phys.* 82 (1985) 299.
- [21] (a) V.A. Rassolov, M.A. Ratner, J.A. Pople, P.C. Redfern, L.A. Curtiss, *J. Comput. Chem.* 22 (2001) 976;  
(b) M.M. Francl, W.J. Pietro, W.J. Hehre, J.S. Binkley, D.J. Defrees, J.A. Pople, M.S. Gordon, *J. Chem. Phys.* 77 (1982) 3654;  
(c) P.C. Hariharan, J.A. Pople, *Mol. Phys.* 27 (1974) 209;  
(d) P.C. Hariharan, J.A. Pople, *Theor. Chim. Acta* 28 (1973) 213;  
(e) W.J. Hehre, R. Ditchfield, J.A. Pople, *J. Chem. Phys.* 56 (1972) 2257.
- [22] (a) G.A. Petersson, M.A. Al-Laham, *J. Chem. Phys.* 94 (1991) 6081;  
(b) G.A. Petersson, A. Bennett, T.G. Tensfeldt, M.A. Al-Laham, W.A. Shirley, J. Mantzaris, *J. Chem. Phys.* 89 (1988) 2193.
- [23] N.M. O'Boyle, A.L. Tenderholt, K.M. Langner, *J. Comput. Chem.* 29 (2008) 839.
- [24] (a) M. Cossi, N. Rega, G. Scalmani, V. Barone, *J. Comput. Chem.* 24 (2003) 669;  
(b) V. Barone, M. Cossi, *J. Phys. Chem. A* 102 (1998) 1995.
- [25] (a) S. Delgado, A. Gallego, O. Castillo, F. Zamora, *Dalton Trans.* 40 (2011) 847;  
(b) M. Du, Y.M. Guo, X.H. Bu, J. Ribas, M. Monfort, *New J. Chem.* 26 (2002) 939;  
(c) M.M. Kimani, D. VanDerveer, J.L. Brumaghin, *Acta Crystallogr.* C67 (2011) m208;  
(d) A.N. Papadopoulos, V. Tangoulis, C.P. Raptopoulou, A. Terzis, D.P. Kessissoglou, *Inorg. Chem.* 35 (1996) 559.
- [26] (a) A. Skorobogaty, T.D. Smith, G. Dougherty, J.R. Pilbrow, *J. Chem. Soc. Dalton Trans.* (1985) 651;  
(b) A.D. Toy, M.D. Hobday, P.D.W. Boyd, T.D. Smith, J.R. Pilbrow, *J. Chem. Soc. Dalton Trans.* (1973) 1259;  
(c) A.D. Toy, T.D. Smith, J.R. Pilbrow, *J. Chem. Soc. Dalton Trans.* (1973) 2498;  
(d) P.D.W. Boyd, A.D. Toy, T.D. Smith, J.R. Pilbrow, *J. Chem. Soc. Dalton Trans.* (1973) 1549;  
(e) J.H. Price, J.R. Pilbrow, K.S. Murray, T.D. Smith, *J. Chem. Soc. A* (1970) 968;  
(f) P.D.W. Boyd, J.R. Pilbrow, T.D. Smith, *Aust. J. Chem.* 24 (1971) 59.